Pore Formation by a Bax-Derived Peptide: Effect on the Line Tension of the Membrane Probed by AFM

Ana J. García-Sáez,* Salvatore Chiantia,* Jesús Salgado,† and Petra Schwille*
*Biotechnologisches Zentrum der TU Dresden, Dresden, Germany; and †Instituto de Ciencia Molecular, Universitat de València, Burjassot, Spain

ABSTRACT Bax is a critical regulator of physiological cell death that increases the permeability of the outer mitochondrial membrane and facilitates the release of the so-called apoptotic factors during apoptosis. The molecular mechanism of action is unknown, but it probably involves the formation of partially lipidic pores induced by Bax. To investigate the interaction of Bax with lipid membranes and the physical changes underlying the formation of Bax pores, we used an active peptide derived from helix 5 of this protein (Bax-α5) that is able to induce Bax-like pores in lipid bilayers. We report the decrease of line tension due to peptide binding both at the domain interface in phase-separated lipid bilayers and at the pore edge in atomic force microscopy film-rupture experiments. Such a decrease in line tension may be a general strategy of pore-forming peptides and proteins, as it affects the energetics of the pore and stabilizes the open state.

INTRODUCTION

Alteration of the permeability of the outer mitochondrial membrane (OMM), a key step in apoptosis, is controlled by proteins of the Bcl-2 family (1). It involves the formation of a pore that allows the release of apoptotic factors, including cytochrome *c*, which, once in the cytosol, promote caspase activation and cell death (2). At this initial stage, the overall integrity of mitochondria is maintained to supply the energetic requirements of the apoptotic pathway. Despite intense research, the nature of the apoptotic pore remains unknown, though evidence shows that cell-death inducers of the Bcl-2 family, like Bax and Bak, are required for the mitochondrial activation loop of apoptosis (3,4).

Bax is soluble in the cytosol under normal conditions. In the presence of apoptotic stimuli, it translocates to the OMM and induces cytochrome *c* release. This process is induced by Bcl-2 members of the BH3-only subgroup, like Bid or PUMA (5,6). At the molecular level, Bax activation is characterized by its targeting to mitochondria, extensive conformational reorganization, and insertion into the OMM. Once there, Bax forms oligomers that induce the release of cytochrome *c* (7–11).

The pore-forming activity that is attributed to Bax has been demonstrated in vitro. At nanomolar concentrations, this protein permeabilizes large unilamellar vesicles (LUVs) to cytochrome *c* and dextrans of high molecular weight (12). It also produces pores in planar supported bilayers, as revealed in atomic force microscopy (AFM) studies (13). Such an activity is affected by the presence of lipids with intrinsic monolayer curvature (14). These facts, together with the properties of Bax-induced ion channels in planar lipid bilayers, led Basanez et al. to propose that Bax forms pores of mixed lipidic/proteic nature (15).

The formation of protein/lipid pores with similar characteristics has also been attributed to other cell-death-related proteins. Examples are colicins (16), actinoporins (17,18), and a number of antimicrobial peptides, like melittin (19) and magainin (20,21). The pore model often proposed in these cases is an idealized toroidal arrangement with the rim of the pore being formed by both lipid and protein molecules. Such nonlamellar structures are characterized by a membrane edge at the pore wall. There, the two monolayers are in contact and form a continuous sheet with positive monolayer curvature in the plane perpendicular to the membrane and negative curvature in the membrane plane (18,21). In the context of this model, the pore-inducing polypeptides are thought to be embedded in the polar surface of the membrane with variable insertion into the hydrocarbon region. Similar pores form in pure lipid bilayers under stress conditions (22). The energetics and dynamics of these lipid pores can be explained by theoretical models (23,24) in which the energy E_r of a pore of radius r is given by

$$E_r = \Gamma 2\pi r - \sigma\pi r^2. \quad (1)$$

Here, the first term represents the energy necessary to expand the rim of the pore, Γ being the line tension at the pore rim. The second term represents the work done by the membrane to open the pore, which is proportional to the pore area, with σ being the membrane tension. This model predicts an intrinsically unstable pore, that tends to close when $r < \Gamma/\sigma$, but expands indefinitely when $r > \Gamma/\sigma$. Assuming that the same physics apply to polypeptide-induced toroidal pores, the action of these molecules should in some way affect the line-tension and membrane-tension terms, making the open-pore state energetically favored (25).

Submitted November 2, 2006, and accepted for publication February 21, 2007.

Address reprint requests to Petra Schwille, Tatzberg 47-51, 1307 Dresden, Germany. Tel.: 49-351-4634-0328; E-mail: petra.schwille@biotec.tu-dresden.de.

Editor: Antoinette Killian.

0006-3495/07/07/103/10 $2.00

doi: 10.1529/biophysj.106.100370

At the molecular level, the pore activity of Bax can be connected to details of its structure. In its water-soluble form, Bax contains a hydrophobic hairpin of α-helices that is buried in the core of the protein (26). By analogy with structurally related proteins, like the pore-forming domain of colicin E1 (27,28), this central hairpin is regarded as the pore-forming domain in Bax. In addition to this, as we have shown, peptides derived from each of the helices in the hydrophobic hairpin can independently reproduce important characteristics of the permeabilizing activity of the full-length parent protein (29,30). This allows us to investigate the physical basis of the pore-forming activity of Bax using reduced systems made of single membrane-active helical fragments.

The aim of this work was to measure the effect of a pore-forming peptide including helix 5 of Bax (Bax-α5) on the properties of lipid membranes. Confocal microscopy and AFM images show characteristic shape changes in domain-exhibiting supported bilayers in the presence of Bax-α5, which are interpreted as a reduction of the line tension at the boundaries of phases. Line tension reductions are also observed from punch-through AFM experiments. These findings support the toroidal pore model as the mechanism of action of Bax-α5.

MATERIALS AND METHODS

Peptide synthesis and purification

The peptides encompassing the helix-5 fragments of the soluble form of Bax (Bax-α5, sequence Ac-DGNFNWGRVVALFYFASKLVLKALSTKVPE-LIRT-NH_2) and the homologous antiapoptotic protein Bcl-xL (Bcl-xL-α5, sequence Ac-RDGVNWGRIVAFFSFGGALSVESVDKEMQVLVSR-NH_2) were chemically synthesized. The only difference between these peptides and the corresponding natural sequences Bax and Bcl-xL from mouse is the replacement of Cys residues by Ser, to avoid dimerization via disulfide bridges.

Solid-phase synthesis of the peptides was carried out as reported (30) in a 433A peptide synthesizer (Applied Biosystems, Foster City, CA) using Fmoc chemistry and Tentagel S-RAM resin (Rapp Polymere, Tübingen, Germany; 0.24 mEq/g substitution) as a solid support. A sixfold molar excess of amino acids (Senn Chemicals, Dielsdorf, Switzerland) was used and multiple couplings were applied on difficult residues (31). The peptides were acetylated at the N-terminus and amidated at the C-terminus. Deprotection and cleavage reactions were performed in a mixture of 70% trifluoroacetic acid, 20% dichloromethane, 5% water, 2.5% triisobutilsylaen, and 2.5% ethanedithiol (v/v), all from Merck. Purification of the peptides was carried out using a C18 preparative reverse-phase column (Merck, Darmstadt, Germany) by high-performance liquid chromatography, to a purity of ~95%, and their identity was confirmed by mass spectrometry. Unless otherwise indicated, all reagents and solvents in the solid-phase synthesis were from Applied Biosystems.

All peptide concentrations were determined from ultraviolet spectra using a Jasco spectrophotometer (Jasco, Tokyo, Japan).

Preparation and size measurement of lipid vesicles

All lipids used were from Avanti Polar Lipids (Alabaster, AL). Large unilamellar vesicles (LUVs) were prepared as described previously (32). Lipids were mixed at the desired molar composition in chloroform and vacuum-dried. Subsequently, they were resuspended to a concentration of 4 mg/mL in a calcein solution. After six cycles of freezing and thawing, they were passed 31 times through two stacked polycarbonate filters of 100-nm pore size, using a two-syringe extruder from Avestin (Ottawa, Canada). To remove external nonencapsulated dye, LUVs were washed in Sephadex-G50 (Sigma-Aldrich, St. Louis, MO) minicolumns, previously equilibrated in 140 mM NaCl, 20 mM Hepes, 1 mM EDTA, pH 7. The size of vesicles was measured by quasielastic light scattering with a laser particle sizer (Malvern Z-sizer 3, Malvern, UK).

Membrane permeability

The permeabilizing activity of the peptides was assayed by measuring the release of calcein from LUVs. All experiments were done at room temperature. A 96-well microtiter plate was filled with the desired amount of peptide and LUVs (final lipid concentration 2–5 mg/mL). The time course of calcein release was measured as the increase in fluorescence emission at 520 nm with the excitation set at 495 nm, using a fluorescence microplate reader (Fluostar, BMG, Munich, Germany). The percentage of peptide-induced calcein release (%R) was calculated by:

$$\%R = 100(F_f - F_i)/(F_m - F_i), \quad (2)$$

where F_f is the value of fluorescence measured after 1 h reaction, F_i is the background fluorescence in the absence of the peptide, and F_m is the maximal fluorescence obtained in the presence of 1 mM Triton X-100. The spontaneous release of calcein was negligible in all cases.

Preparation of planar supported bilayers

Planar supported bilayers were prepared following the protocol described in Chiantia et al. (33). Lipids were dissolved in chloroform at the desired molar concentration and 1,1′-dioctadecyl-3,3,3′,3′-tetramethylindodicarbocyanine perchlorate (DiD-C18) (Molecular Probes, Eugene, OR) was added to the lipid mixtures at a 0.01% (mol/mol) concentration. The solvent was evaporated under nitrogen flux and then subjected to vacuum for 1 h. Lipid mixtures were rehydrated to a final concentration of 10 mg/mL in 3 mM KCl, 1.5 mM KH_2PO_4, 8 mM Na_2HPO_4, and 150 mM NaCl, pH 7.2. The suspension was then vortexed and bath-sonicated at 60° until small unilamellar vesicles were obtained. A small aliquot of the small-unilamellar-vesicle suspension (10 μl) was diluted in 140 μl of 3 mM $CaCl_2$, 150 mM NaCl, 10 mM Hepes, and 3 mM NaN_3, pH 7.4, and then put in contact with freshly cleaved mica substrate, previously glued to a glass coverslip. The mixture was incubated at 40°C for 2 min, and then at 65°C for 10 min. The samples were rinsed several times with 150 mM NaCl, 10 mM Hepes, and 3 mM NaN_3, pH 7.4, to remove the nonfused vesicles, and then were allowed to cool down and equilibrate for 1 h. The lipid content per sample was ~2 nmol, calculated assuming an average area/ lipid molecule of 0.6 nm^2 (34).

Confocal microscopy

Confocal fluorescence microscopy was performed on a LSM Meta 510 instrument (Carl Zeiss, Jena, Germany). Confocal images were taken using the excitation light of an He-Ne laser at 633 nm, which was reflected by a dichroic mirror (HTF 488/633) and focused through a Zeiss C-Apochromat 40×, NA 1.2, water-immersion objective onto the sample. The fluorescence signal was collected by the same objective, passed through a 680/30 nm bandpass filter, and finally detected by a photomultiplier. Confocal geometry was ensured by a 90-μm pinhole in front of the photomultiplier.

AFM measurements

AFM measurements were performed using a NanoWizard system (JPK Instruments, Berlin, Germany) mounted on the same LSM Meta 510 setup

used for microscopy. Contact-mode topographic images were taken in the constant-deflection mode, using V-shaped silicon nitride cantilevers (Veeco, Santa Barbara, CA) with a typical spring constant of 0.08 N m^{-1}. The force applied on the sample was maintained at the lowest possible value by continuously adjusting the set point during imaging. The scan rate was set between 1 and 2 Hz. Height and deflection were collected simultaneously in both trace and retrace directions. Images were line-fitted as required. Occasionally, isolated scan lines were removed.

For force measurements, the calibration of sensitivity, resonance frequency, and effective spring constant (via the thermal noise method) (35) of the cantilever were performed before and after each experiment. The total z-piezo displacement was always 300 nm and the indenting speed was set to 800 nm/s for the approach and 200 nm/s for the retraction. All experiments were carried out at different positions of the bilayer under the same conditions, so that the effect of speed on the breakthrough force could be neglected. The approach curves were analyzed using the free software Punias (P. Carl and P. Dalhaimer, 2004) and the threshold yield was measured for 150–400 different curves in each sample and plotted in histograms as in Garcia-Manyes et al. (36).

Continuum nucleation model for the rupture of thin films

Based on the continuum nucleation theory, Butt et al. described a theoretical model that relates the yield force of film rupture to microscopic properties of the bilayer (37). In their model, the rupture of a fluid film is considered an activated process, with an associated energy barrier that follows the Arrhenius law:

$$k(t) = Ae^{-\Delta U(t)/k_B T}, \tag{3}$$

where A is a frequency factor and $\Delta U = U_f - U_i$ is the energy difference of the film before (U_i) and after (U_f) rupture. The energy of the system at U_i increases with the applied force due to the pressure produced by the tip on the bilayer.

The differential equation for the kinetics of film rupture is $dN = -kNdt$, where N is the number of times that the tip is on top of an intact film. Dividing by the total number of times that the tip tries to puncture the bilayer N_0, we change to probabilities:

$$dP = -k(t)Pdt, \tag{4}$$

where $P = N/N_0$ is the probability of finding the AFM tip on top of an intact film. This differential equation can be integrated, so that

$$\ln P(t) = -\int_{t_S}^{t} k(t')dt' \quad \text{for} \quad t > t_S, \tag{5}$$

where t_S is the ''starting time'', or the time at which the force applied by the tip has increased the energy of the system to $U_i > U_f$. For $t \le t_S$, the film will not break and $P = 1$.

To express the probability of rupture in terms of force instead of time, some considerations must be taken. The force is zero until the tip contacts the film. Then, since the tip moves toward the sample with a constant speed v, after contact the force is $F = Kvt$, where K is the spring constant of the cantilever. As a result,

$$\ln P(F) = \frac{A}{Kv}\int_{F_S}^{F} e^{-\Delta U(F')/k_B T}dF' \quad \text{for} \quad F > F_S, \tag{6}$$

where $F_S = Kvt_S$ is the ''starting force''.

According to the continuum nucleation model (see Eq. 1), and for a system composed by a supported bilayer pressed by an AFM tip of radius R, the energy of a pore of radius r_h is given by

$$U = 2\pi r_h\Gamma + \pi r_h^2\left(S - \frac{F}{2\pi R}\right). \tag{7}$$

The linear factor depends on the line tension Γ at the generated membrane edge, whereas the surface factor depends on a term S, called spreading pressure, and on the elastic energy of the confined film. In our system, the spreading pressure includes the interactions between the different interfaces involved in the punch-through process (tip, liquid solution, lipid bilayer, and solid support).

The elastic energy is stored in the film upon compression by the AFM tip, and it is released when a pore of radius r_h forms. The contribution of the elastic energy is calculated using the elastic foundation model, where the indentation of the AFM tip of radius R at a radial position r is given by

$$\delta = \delta_0 - \frac{r^2}{2R}, \tag{8}$$

valid for $r \le a = \sqrt{2\delta_0 R}$, with a being the peripheral radius of the contact area. The elastic force equation, $F = EA_r\delta/h$, where E is the Young modulus, A_r is the area through which the force is applied, h is the thickness of the film, and δ is the indentation, can be integrated over the radial position r. It relates the maximal indentation in the center δ_0 and the applied force F by

$$\delta_0 = \sqrt{\frac{hF}{\pi ER}}. \tag{9}$$

Then, the elastic energy U_e stored in a small section of the film of radius r_h can be expressed as a function of applied force:

$$U_e = \frac{E\pi r_h^2\delta_0^2}{2h} = \pi r_h^2\frac{F}{2\pi R}. \tag{10}$$

Equation 7, for the energy of a hole of radius r_h, shows a maximum at a critical radius:

$$r_C = \frac{2\pi R\Gamma}{F - 2\pi RS}. \tag{11}$$

Then, the maximal energy, which is the activation energy, is given by

$$\Delta U = U(r_C) = \frac{2\pi^2\Gamma^2 R}{F - 2\pi RS}. \tag{12}$$

Substitution of Eq. 12 in Eq. 6 leads to an expression for the probability $P(F)$ of measuring a certain threshold yield F of film rupture, which is described by

$$\ln P(F) = -\frac{A}{K\nu}\int_{F_S}^{F}\exp\left(-\frac{c}{F' - F_S}\right)dF',$$
$$\text{with} \quad c = \frac{2\pi^2\Gamma^2 R}{k_B T} \quad \text{and} \quad F_S = 2\pi RS, \tag{13}$$

where A is the frequency factor, ν is the loading rate, k_B is the Boltzmann constant, T is the temperature, and K is the spring constant of the cantilever (38). Equation 13 can be integrated analytically and dP/dF can be calculated (39):

$$\frac{dP}{dF} = \frac{A}{K\nu}\exp\left(-\frac{c}{F - F_S} - \frac{A}{K\nu}\left(\exp\left(-\frac{c}{F - F_S}\right)\right.\right.$$
$$\left.\left.\times (F - F_S) - c\,\mathrm{Ei}\left(\frac{c}{F - F_S}\right)\right)\right) \tag{14}$$
$$\mathrm{Ei}(x) = \int_x^{\infty} e^{-t}/t\,dt.$$

In a punch-through experiment, the unknown parameters in Eq. 14 are the frequency factor A, the line tension Γ at the pore edge, and the spreading

pressure *S*. They can be calculated by fitting this equation to the measured-yield histograms.

RESULTS AND DISCUSSION

Bax-α5 affects the morphology of lipid domains in supported bilayers

Supported bilayers made of phosphatidylcholine:sphingomyelin:cholesterol (PC/SM/Chol) (1:1:0.67) exhibit two coexisting phases: The first one is enriched in SM and Chol, shows short-range order, and is commonly known as liquid-ordered phase (L_o). The second phase is enriched in dioleoylphospatidylcholine (DOPC) and is liquid-disordered (L_d). Phase separation induces the formation of large domains of a few micrometers, which can be visualized by confocal fluorescence microscopy. As shown in Fig. 1, the lateral distribution of the fluorescent dye DiD is heterogeneous, since it is excluded from the ordered domains (*dark patches*) (33).

The circular morphology of the L_o domains in the absence of Bax-α5 (control conditions, Fig. 1, *top left*) indicates the existence of line tension between the two phases. This appears to be due to the chemical inhomogeneity and the different thickness at the boundary of the coexisting domains, which leads to lipid tilt and curvature stress (40,41).

When Bax-α5 is added at a lipid/protein (*L*/*P*) molar ratio of 109, a dramatic change in the morphology of the L_o domains is observed: they become more irregular and larger (Fig. 1, *time series*). The kinetics of the process is fast: It starts immediately after adding the peptide, and equilibrium is reached within 10 min. The analysis of the lipid-supported bilayers under similar conditions by scanning AFM allows imaging at a higher resolution. In Fig. 2 *A*, pure DOPC/SM/Chol (1:1:0.67) membranes in equilibrium exhibit numerous round L_o domains, with diameters in the range 0.5–3 μm. The ordered domains are thicker than the surrounding disordered phase, with a height difference between the two phases of ~0.7 nm. As shown above, in the presence of Bax-α5 at $L/P = 109$ (Fig. 2 *C*), the domains become irregular. Overall, there are fewer domains and they are bigger, though their diameter is difficult to estimate because of the complex shape.

These results reveal a decrease in the line tension at the phase boundary in the presence of the Bax peptide. A similar effect on domain shape was observed in domain exhibiting vesicles when the temperature was raised close to the phase transition temperature T_m, and was also interpreted as a drop of line tension (42). The domain interface contains a higher concentration of packing defects, which are expected to favor Bax-α5 binding because of its amphipathic nature (43). There, the peptide may stabilize the tensed domain boundary by releasing stress of curvature and thus reducing the line tension (44). Such an effect may be common to similar types of molecules, like antimicrobial peptides, the pore-forming domain of bacterial toxins or detergents (45). In agreement with this idea, Huang et al. proposed a model in which pore-forming peptides stabilize the open state through a decrease in the line tension (25).

As a control experiment, we performed similar measurements in the presence of the peptide Bcl-xL-α5. This peptide is derived from helix 5 of protein Bcl-xL, an antiapoptotic member of the Bcl-2 family. Despite their opposing activities, Bcl-xL and Bax show similar soluble structures, and their

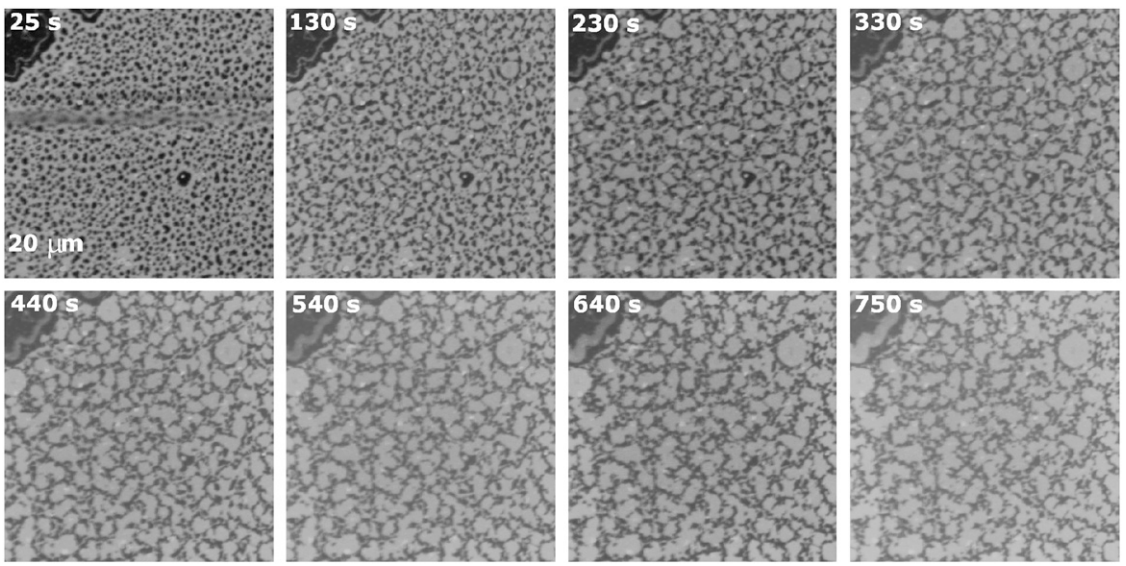

FIGURE 1 Kinetics of the morphological changes induced by Bax-α5 in domain-exhibiting membranes. Bax-α5 was added to DOPC/SM/Chol (1:1:0.67) supported bilayers containing 0.01% DiD to $L/P = 109$ 25 s after the film starts. Confocal images were taken at 25-s intervals for 10 min. The selected times are shown.

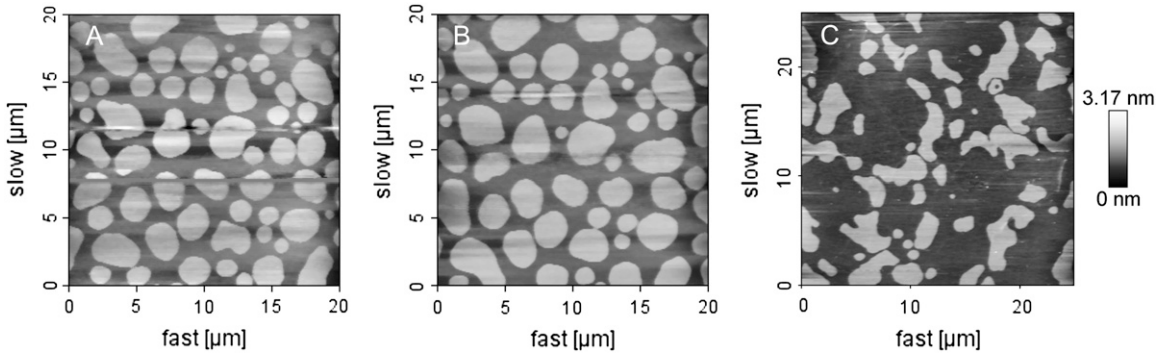

FIGURE 2 AFM topographical images of supported lipid bilayer composed of DOPC/SM/Chol (1:1:0.67) and imaged at 25°C. Bright and dark regions represent SM-rich and DOPC-rich phases, respectively. (*A*) AFM topographical appearance of a freshly prepared supported membrane at equilibrium. (*B*) The same supported bilayer as in *A*, but 1 h after addition of Bcl-xL-α5 at $L/P = 14$ molar ratio. (*C*) Surface of a supported bilayer with the same lipid composition as in *A*, but 30 min after addition of Bax-α5 at $L/P = 109$ molar ratio.

helix 5 fragments show a high level of sequence homology (26,46,47) (see details of the sequences in Materials and Methods). Although there are small differences between the two peptides, Bcl-xL-α5 shows a barely detectable membrane poration activity at neutral pH (A. J. García-Sáez and J. Salgado, unpublished results), which contrasts with the high activity of Bax-α5. Therefore, the Bcl-xL-α5 peptide constitutes a good control for the Bax-α5 experiments. After treating domain exhibiting bilayers with Bcl-xL-α5, no significant changes in the domain shape, size, or thickness were observed in confocal microscopy or AFM images for *L/P* molar ratios up to 14 and 1 h incubation (Fig. 2 *B*). These results demonstrate that the effects observed in the presence of Bax-α5 are due to specific peptide/lipid interactions arising from the physicochemical properties coded in the sequence of the peptide.

Bax-α5 decreases the force needed to rupture the membrane in a two-step process

To investigate whether Bax-α5 had an effect on the mechanical properties of the membrane, we collected a statistically significant number of force-distance curves in the L_d and L_o phases at several peptide concentrations, and measured the force required for the AFM tip to punch through the membrane. In this kind of measurement, the tip of the cantilever is moved toward the sample. The force-distance curves represent the deflection of the cantilever as a function of the position of the tip. Fig. 3 shows a typical force curve obtained when measuring on supported lipid bilayers. When a certain yield force is exceeded, a jump is often observed, which is interpreted as a penetration of the AFM tip through the bilayer (37). A distribution of punch-through values is obtained and is plotted in a histogram.

The histograms of experimental yield forces measured for bilayers composed of pure DOPC/SM/Chol (1:1:0.67) are depicted in Fig. 4 *A*. The average force needed to break through the bilayer in the L_o domains is ~8 nN, higher than that in the L_d domains (~5 nN). This is in agreement with the physical properties of the two bilayer phases, with the ordered L_o phase being less fluid and more compressed (as previously shown in Chiantia et al. (39)).

In the presence of low concentrations of the Bax-α5 peptide ($L/P = 109$ and $L/P = 54$), where morphological changes are clearly observed (see Figs. 1 and 2), the forces required to punch through the membranes become similar for the two phases (Fig. 4, *B* and *C*). In this concentration range, the punch-through force increases with the peptide concentration. However, past a threshold *L/P* value close to 27, the force required to make a hole in any of the phases decreases drastically to around 1 nN, indicating changes in the mechanical properties of the bilayer (Fig. 4, *D* and *E*). These

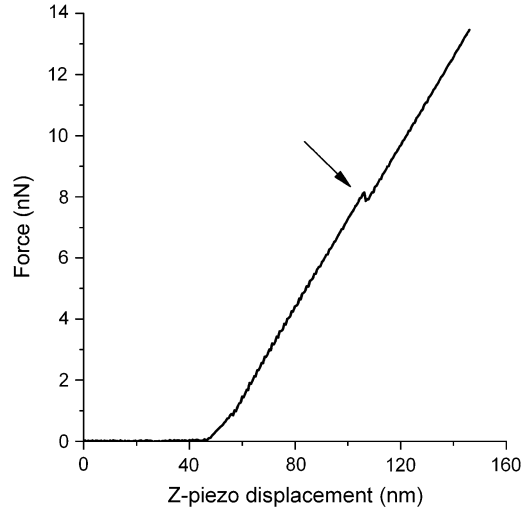

FIGURE 3 Typical approach part of a force curve measured on the L_o domain in a DOPC/SM/Chol (1:1:0.67) supported bilayer on mica. The force applied by the cantilever is represented as a function of the *z*-piezo displacement. The discontinuity in the curve corresponds to the yield force required for the AFM tip to punch through the bilayer (*arrow*).

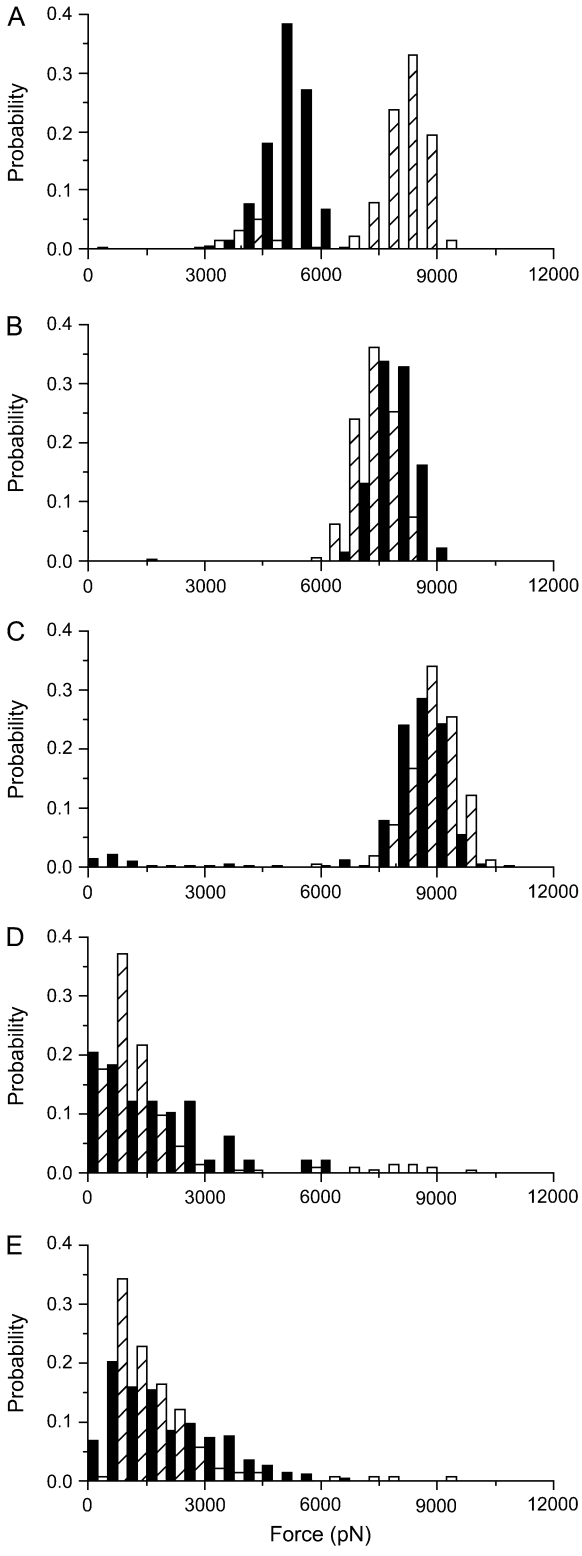

FIGURE 4 Histograms of yield forces measured on a DOPC/SM/Chol (1:1:0.67) bilayer at different Bax-α5 concentrations: (*A*) in the absence of peptide; (*B*) at $L/P = 109$; (*C*) at $L/P = 55$; (*D*) at $L/P = 27$; and (*E*) at $L/P = 14$. The black bars correspond to the L_d phase, whereas the dashed bars correspond to the L_o phase. The histograms are normalized for better comparison (the number of points varied between 70 and 350).

results show two states in the Bax-α5 interaction with the lipid bilayer, depending on the peptide concentration, in agreement with the behavior observed for membrane permeability (30). Besides, the distribution of the histograms is wider in the presence of the peptide, which suggests that Bax-α5 is heterogeneously distributed in the membrane.

When we measured the yield forces to punch through the L_o and L_d phases in the presence of the control peptide Bcl-xL-α5 up to $L/P = 14$, the distributions of forces remained practically unchanged compared to pure bilayers (Fig. 5). At the highest concentrations measured (Fig. 5 *C*), only a slight increase in the punch-through force was detected for the L_d phase. However, and in contrast to the results obtained for Bax-α5, neither reduction of the piercing force nor two-state behavior could be measured for Bcl-xL-α5. The membrane was stable under the measuring conditions in all experiments, as confirmed by confocal microscopy and/or AFM imaging.

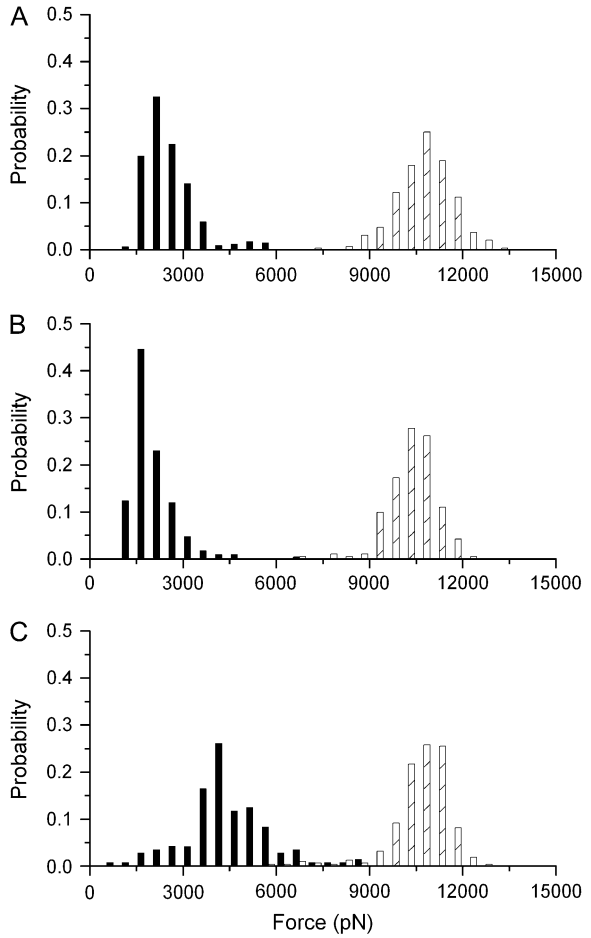

FIGURE 5 Histograms of yield forces measured on a DOPC/SM/Chol (1:1:0.67) bilayer at different Bcl-xL-α5 concentrations: (*A*) in the absence of peptide; (*B*) at $L/P = 55$; and (*C*) at $L/P = 14$. The black bars correspond to the L_d phase, whereas the dashed bars correspond to the L_o phase. The histograms are normalized for better comparison (the number of points varied between 70 and 350).

Bax-α5 decreases the line tension at the rim of the pore

To reduce the complexity of the system for a quantitative analysis, we measured force curves in palmitoyloleoylphosphatidylcholine (POPC) bilayers at different Bax-α5 concentrations (Fig. 6). In the absence of peptide, the average force to disrupt the bilayer is ~4 nN, thus similar to that corresponding to the L_d phase in raftlike bilayers, and in agreement with the fluid state of the membrane (Fig. 6 *A*). In line with the results just discussed, the presence of the peptide above a certain concentration induces a drop in the yield force needed for punch-through, as compared to pure POPC bilayers. In this case, a two-step behavior is also observed, but the threshold *L*/*P* for the characteristic decrease of force is much lower than in DOPC/SM/Chol (1:1:0.67) bilayers, being ~5000 (Fig. 6 *B*). This is consistent with the permeabilizing activity measured in LUVs, which is notably higher in PC vesicles than in LUVs with raftlike composition (Fig. 7).

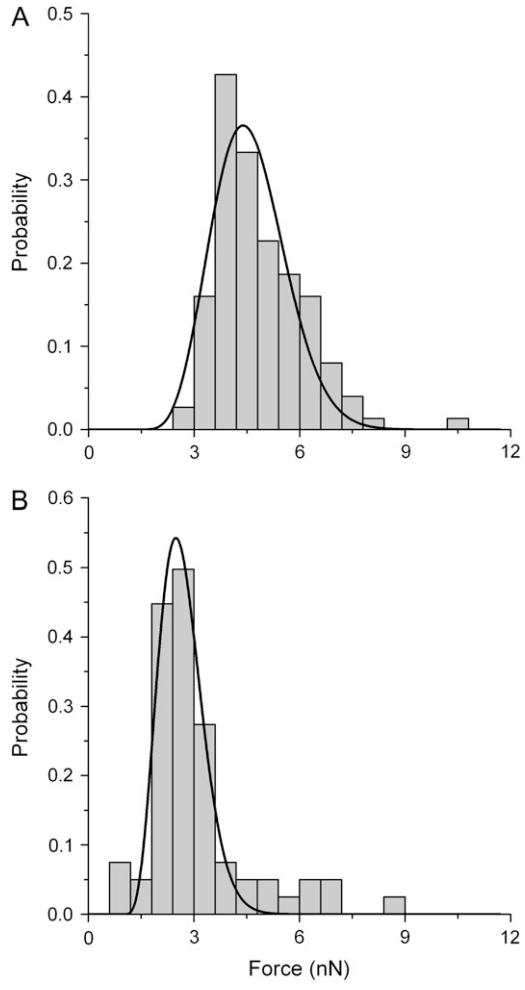

FIGURE 6 Normalized histograms of yield forces measured on a POPC supported bilayer (*A*) in the absence and (*B*) at a ratio of $L/P \approx 5000$ of Bax-α5. The solid lines correspond to the fitted function of probability density from Eq. 14. The number of points was 66 in *A* and 124 in *B*.

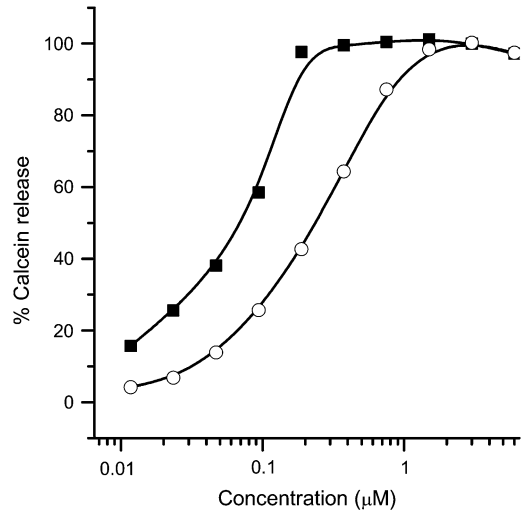

FIGURE 7 Permeabilizing activity of Bax-α5 in LUVs. The percentage of calcein release, according to Eq. 2, is represented as a function of the concentration of added peptide. Vesicles were composed of egg PC (*solid squares*) or PC/SM/Chol (1:1:1) (*open circles*).

To fit the force histograms to Eq. 14 (see Materials and Methods), we used a nominal curvature radius for the tip, *R*, of 50 nm, and we measured the spring constant of the cantilever, *K*, which was found to be ~0.15 N/m. We started the fitting procedure by choosing a certain value of frequency factor, *A* (37,39). The best results were obtained for $A = 1$ kHz, although using other values of *A* did not significantly affect the relationship between the fitted parameters in the absence and the presence of peptide. Table 1 shows the values obtained for the line tension and the spreading pressure after fitting the histograms in Fig. 6.

The line tension obtained for pure POPC bilayers, $\Gamma = 6.0 \pm 0.3$ pN, is in line with results published previously for DOPC bilayers (~3.9 and ~6.9 pN) (1,39,43). Addition of Bax-α5 reduces the line tension at the rim of the pore by ~30% (Table 1), similar to the effect observed in the presence of detergents (43,45).

Interpretation in the framework of the pore activity

Similar to antimicrobial peptides, like melittin and magainin, the active Bax-α5 fragment is an amphipathic α-helix with

TABLE 1 Estimated line tension, Γ, and spreading pressure, *S*, in POPC supported bilayers in the presence and absence of Bax-α5

Bax-α5	Γ(pN)	S *(mN/m)*
0	6.0 ± 0.3	3 ± 3
$L/P \approx 5000$	3.8 ± 0.4	2.4 ± 0.9

Results were obtained by fitting the force histograms in Fig. 6 to Eq. 14, with a value of $A = 1$ kHz. The indicated errors correspond to 2σ obtained in the fitting.

net positive charge provided by lysine and arginine residues. For this type of molecule, it is generally proposed that binding occurs at the bilayer interface between the headgroup and the hydrophobic region (21,30,45,48). Such a binding mode would insert additional area into the polar region and provoke deformations and stress in the bilayer. According to the two-state model proposed by Huang et al. (25), the pore state occurs after a threshold concentration of the peptide is bound to the membrane, and the built-up stress is sufficient to allow formation of a pore. In the open pore, a reduced line tension due to peptide binding may change the energetic balance (see Eq. 1) and increase the stability of the pore state.

Our results show that the pore-forming peptide Bax-α5 reduces the line tension at interfaces with high curvature stress, as in domain boundaries and mechanically punched holes. The concentration-dependent two states displayed by the Bax-α5/membrane interaction in punch-through experiments is in agreement with the cooperative pore-forming activity of the same peptide measured by the release of contents from LUVs (Fig. 7). Indeed, for a raftlike lipid composition of LUVs, 50% of activity is reached at an $L/P = 17$, which is in the same order of magnitude as the L/P values necessary for the step reduction of punch-through forces. This behavior agrees with Huang's two-state model (49). At low L/P ratios Bax-α5 binds to the membrane, most probably at the level of the interface (Fig. 8, *2*). This would introduce additional area into the lipid headgroup region, thus increasing the lateral pressure and the force required for the AFM tip to punch through the membrane. Since the L_d phase is less packed than the L_o phase, more peptide molecules may bind to it (50), which would explain the stronger increase in the observed yield force for L_d. The effect at high concentrations corresponds to the state of pore formation (Fig. 8, *3*). In these conditions, Bax-α5 reduces the energy required for punching through, probably by inducing holes in the membrane, which may facilitate the penetration of the tip. This makes sense, since the diameter of the pores induced by Bax-α5 is estimated to be $\sim$5 nm (29), whereas the diameter of the tip is in the order of 50 nm. Fitting Eq. 14 to experimental data shows that Bax-α5 produces a reduction of the line tension under conditions corresponding to state 3 in Fig. 8 (above the threshold concentration). This effect is an important factor for the stability of the peptide-induced pore. Such a reduction of line tension reflects a release of curvature stress at the membrane edge in the pore wall (Fig. 8, *3*), in a way analogous to the pore-stabilizing curvature effects of detergents (43). This is expected to be a general mechanism for pore stabilization by polypeptides similar to Bax-α5, including the complete Bax protein.

In addition, the time-dependent variation of domain morphology induced by Bax-α5 in DOPC/SM/Chol (1:1:0.67) (Fig. 1) is in good agreement with the time dependence of the peptide activity observed in experiments of content release (29,30). Assuming a similar mechanism for pores made by full-length Bax in mitochondria, they would be long-lived enough to ensure release of the apoptotic factors, which takes $<$10 min in the case of cytochrome *c*, Omi, and Smac, but needs hours in the case of AIF (51).

CONCLUDING REMARKS

In this work, we have evaluated the effect of a pore-forming peptide derived from helix 5 of Bax on the line tension, one of the critical mechanical properties of the lipid bilayer governing pore formation and stability. We report that Bax-α5 affects the morphological organization of domain-exhibiting membranes, as observed by both confocal microscopy and scanning AFM. The peptide reduced the line tension between the two coexisting phases, and therefore, the liquid-ordered domains lost their circular shape and generally increased in size. In addition, force spectroscopy AFM measurements showed that the force needed to punch through lipid bilayers in the presence of Bax-α5 decreased, in agreement with the two-state model of pore formation. To our knowledge, this is the first time force spectroscopy AFM has been used to investigate the molecular mechanism of pore formation in lipid bilayers. Fitting these results to a model based on the continuum nucleation theory yielded a reduction of $\sim$30% in the pore line tension in the presence of the peptide. As Bax-α5 contains the main active fragment of Bax and forms pores with similar properties to the pores of the full-length protein, we propose that a similar effect on the line tension is part of the mechanism of pore formation by the parent Bax. Moreover, because most polypeptides forming toroidal pores in membranes share basic physicochemical properties, we propose that they act via reduction of membrane line tension, as is shown here for Bax-α5.

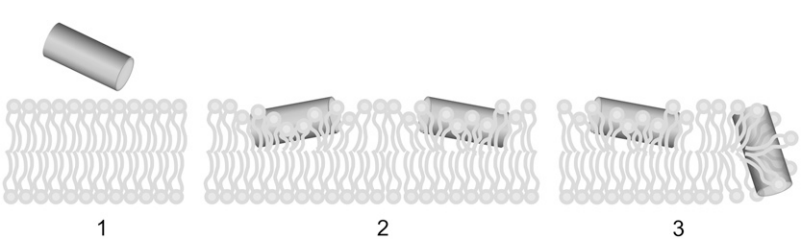

FIGURE 8 Proposed mechanism of pore formation by Bax-α5. Bax-α5 is an amphipathic molecule with hydrophobic residues on one side (*blue*) and net positive charge on the other side (*red*). (*1*) Electrostatic forces favor the interaction with the polar surface of the membrane. (*2*) Insertion of the peptide at the interface between the headgroup region and the hydrophobic region provokes lipid distortion and induces stress in the bilayer. (*3*) After a threshold concentration, Bax-α5 forms pores of a toroidal nature and stabilizes them by reducing the line tension at the pore rim.

We thank Dr. P. H. Puech for helpful discussions, Dr. E. Pérez-Payà for helping with the synthesis and purification of the peptides, J. Suckale for careful reading of the manuscript, and J. Ries for discussion and exceptional support in the fitting procedure. M. Coraiola and M. Dalla Serra are acknowledged for their help with the experiments of contents release.

This work was supported by the Federation of European Biochemical Societies (Short-term fellowship to A.J.G.S.) and grants from the Spanish Ministerio de Educación y Ciencia (CTQ2004-03444) and German Deutsche Forschungsgemeinschaft (SCHW716/4-1) and the Europäische Fonds für Regionale Entwicklung (4212/04-02).

REFERENCES

1. Adams, J. M., and S. Cory. 1998. The Bcl-2 protein family: arbiters of cell survival. *Science*. 281:1322–1326.
2. Newmeyer, D. D., and S. Ferguson-Miller. 2003. Mitochondria: releasing power for life and unleashing the machineries of death. *Cell*. 112:481–490.
3. Wei, M. C., W. X. Zong, E. H. Cheng, T. Lindsten, V. Panoutsakopoulou, A. J. Ross, K. A. Roth, G. R. MacGregor, C. B. Thompson, and S. J. Korsmeyer. 2001. Proapoptotic BAX and BAK: a requisite gateway to mitochondrial dysfunction and death. *Science*. 292:727–730.
4. Zong, W. X., T. Lindsten, A. J. Ross, G. R. MacGregor, and C. B. Thompson. 2001. BH3-only proteins that bind pro-survival Bcl-2 family members fail to induce apoptosis in the absence of Bax and Bak. *Genes Dev*. 15:1481–1486.
5. Crompton, M. 2000. Bax, Bid and the permeabilization of the mitochondrial outer membrane in apoptosis. *Curr. Opin. Cell Biol*. 12:414–419.
6. Ming, L., P. Wang, A. Bank, J. Yu, and L. Zhang. 2006. PUMA dissociates Bax and Bcl-X(L) to induce apoptosis in colon cancer cells. *J. Biol. Chem*. 281:16034–16042.
7. Antonsson, B., S. Montessuit, B. Sanchez, and J. C. Martinou. 2001. Bax is present as a high molecular weight oligomer/complex in the mitochondrial membrane of apoptotic cells. *J. Biol. Chem*. 276:11615–11623.
8. Desagher, S., A. Osen-Sand, A. Nichols, R. Eskes, S. Montessuit, S. Lauper, K. Maundrell, B. Antonsson, and J. C. Martinou. 1999. Bid-induced conformational change of Bax is responsible for mitochondrial cytochrome *c* release during apoptosis. *J. Cell Biol*. 144:891–901.
9. Goping, I. S., A. Gross, J. N. Lavoie, M. Nguyen, R. Jemmerson, K. Roth, S. J. Korsmeyer, and G. C. Shore. 1998. Regulated targeting of BAX to mitochondria. *J. Cell Biol*. 143:207–215.
10. Wolter, K. G., Y. T. Hsu, C. L. Smith, A. Nechushtan, X. G. Xi, and R. J. Youle. 1997. Movement of Bax from the cytosol to mitochondria during apoptosis. *J. Cell Biol*. 139:1281–1292.
11. Yethon, J. A., R. F. Epand, B. Leber, R. M. Epand, and D. W. Andrews. 2003. Interaction with a membrane surface triggers a reversible conformational change in Bax normally associated with induction of apoptosis. *J. Biol. Chem*. 278:48935–48941.
12. Terrones, O., B. Antonsson, H. Yamaguchi, H. G. Wang, J. H. Liu, R. M. Lee, A. Herrmann, and G. Basanez. 2004. Lipidic pore formation by the concerted action of proapoptotic BAX and tBID. *J. Biol. Chem*. 279:30081–30091.
13. Epand, R. F., J. C. Martinou, S. Montessuit, R. M. Epand, and C. M. Yip. 2002. Direct evidence for membrane pore formation by the apoptotic protein Bax. *Biochem. Biophys. Res. Commun*. 298:744–749.
14. Basanez, G., J. C. Sharpe, J. Galanis, T. B. Brandt, J. M. Hardwick, and J. Zimmerberg. 2002. Bax-type apoptotic proteins porate pure lipid bilayers through a mechanism sensitive to intrinsic monolayer curvature. *J. Biol. Chem*. 277:49360–49365.
15. Basanez, G., A. Nechushtan, O. Drozhinin, S. Tutt, K. A. Wood, Y. T. Hsu, R. J. Youle, and J. Zimmerberg. 1999. Studying the mechanism of Bax induced membrane destabilization: does Bax promote lipidic pore formation? *FASEB J*. 13:A1436. (Abstr.)
16. Sobko, A. A., E. A. Kotova, Y. N. Antonenko, S. D. Zakharov, and W. A. Cramer. 2004. Effect of lipids with different spontaneous curvature on the channel activity of colicin E1: evidence in favor of a toroidal pore. *FEBS Lett*. 576:205–210.
17. Anderluh, G., S. M. Dalla, G. Viero, G. Guella, P. Macek, and G. Menestrina. 2003. Pore formation by equinatoxin II, a eukaryotic protein toxin, occurs by induction of nonlamellar lipid structures. *J. Biol. Chem*. 278:45216–45223.
18. Valcarcel, C. A., S. M. Dalla, C. Potrich, I. Bernhart, M. Tejuca, D. Martinez, F. Pazos, M. E. Lanio, and G. Menestrina. 2001. Effects of lipid composition on membrane permeabilization by sticholysin I and II, two cytolysins of the sea anemone *Stichodactyla helianthus*. *Biophys. J*. 80:2761–2774.
19. Yang, L., T. A. Harroun, T. M. Weiss, L. Ding, and H. W. Huang. 2001. Barrel-stave model or toroidal model? A case study on melittin pores. *Biophys. J*. 81:1475–1485.
20. Ludtke, S. J., K. He, W. T. Heller, T. A. Harroun, L. Yang, and H. W. Huang. 1996. Membrane pores induced by magainin. *Biochemistry*. 35:13723–13728.
21. Matsuzaki, K., O. Murase, N. Fujii, and K. Miyajima. 1996. An antimicrobial peptide, magainin 2, induced rapid flip-flop of phospholipids coupled with pore formation and peptide translocation. *Biochemistry*. 35:11361–11368.
22. Sandre, O., L. Moreaux, and F. Brochard-Wyart. 1999. Dynamics of transient pores in stretched vesicles. *Proc. Natl. Acad. Sci. USA*. 96: 10591–10596.
23. Taupin, C., M. Dvolaitzky, and C. Sauterey. 1975. Osmotic pressure induced pores in phospholipid vesicles. *Biochemistry*. 14:4771–4775.
24. Lee, M. T., F. Y. Chen, and H. W. Huang. 2004. Energetics of pore formation induced by membrane active peptides. *Biochemistry*. 43: 3590–3599.
25. Huang, H. W., F. Y. Chen, and M. T. Lee. 2004. Molecular mechanism of Peptide-induced pores in membranes. *Phys. Rev. Lett*. 92:198304.
26. Suzuki, M., R. J. Youle, and N. Tjandra. 2000. Structure of Bax: coregulation of dimer formation and intracellular localization. *Cell*. 103:645–654.
27. Cramer, W. A., J. B. Heymann, S. L. Schendel, B. N. Deriy, F. S. Cohen, P. A. Elkins, and C. V. Stauffacher. 1995. Structure-function of the channel-forming colicins. *Annu. Rev. Biophys. Biomol. Struct*. 24: 611–641.
28. Stroud, R. M., K. Reiling, M. Wiener, and D. Freymann. 1998. Ion-channel-forming colicins. *Curr. Opin. Struct. Biol*. 8:525–533.
29. Garcia-Saez, A. J., M. Coraiola, M. D. Serra, I. Mingarro, P. Muller, and J. Salgado. 2006. Peptides corresponding to helices 5 and 6 of Bax can independently form large lipid pores. *FEBS J*. 273:971–981.
30. Garcia-Saez, A. J., M. Coraiola, S. M. Dalla, I. Mingarro, G. Menestrina, and J. Salgado. 2005. Peptides derived from apoptotic Bax and Bid reproduce the poration activity of the parent full-length proteins. *Biophys. J*. 88:3976–3990.
31. Fisher, L. E., and D. M. Engelman. 2001. High-yield synthesis and purification of an α-helical transmembrane domain. *Anal. Biochem*. 293:102–108.
32. Dalla, S. M., and G. Menestrina. 2003. Liposomes in the study of pore-forming toxins. *Methods Enzymol*. 372:99–124.
33. Chiantia, S., N. Kahya, and P. Schwille. 2005. Dehydration damage of domain-exhibiting supported bilayers: an AFM study on the protective effects of disaccharides and other stabilizing substances. *Langmuir*. 21: 6317–6323.
34. Simons, K., and W. L. C. Vaz. 2004. Model systems, lipid rafts, and cell membranes. *Annu. Rev. Biophys. Biomol. Struct*. 33:269–295.
35. Florin, E. L., M. Rief, H. Lehmann, M. Ludwig, C. Dornmair, V. T. Moy, and H. E. Gaub. 1995. Sensing specific molecular interactions with the atomic force microscope. *Biosens. Bioelectron*. 10:895–901.
36. Garcia-Manyes, S., G. Oncins, and F. Sanz. 2005. Effect of ion-binding and chemical phospholipid structure on the nanomechanics of lipid bilayers studied by force spectroscopy. *Biophys. J*. 89:1812–1826.

37. Butt, H. J., and V. Franz. 2002. Rupture of molecular thin films observed in atomic force microscopy. I. Theory. *Phys. Rev.* 66:031601-1–031601-9.

38. Loi, S., G. Sun, V. Franz, and H. J. Butt. 2002. Rupture of molecular thin films observed in atomic force microscopy. II. Experiment. *Phys. Rev.* 66:031602-1–031602-7.

39. Chiantia, S., Ries, J., Kahya, N., and Schwille, P. 2006. Combined AFM and two-focus SFCS study of raft-exhibiting model membranes. *Chemphyschem.* 7:2409–2418.

40. Akimov, S. A., P. I. Kuzmin, J. Zimmerberg, F. S. Cohen, and Y. A. Chizmadzhev. 2004. An elastic theory for line tension at a boundary separating two lipid monolayer regions of different thickness. *J. Electroanal. Chem.* 564:13–18.

41. Baumgart, T., S. Das, W. W. Webb, and J. T. Jenkins. 2005. Membrane elasticity in giant vesicles with fluid phase coexistence. *Biophys. J.* 89:1067–1080.

42. Baumgart, T., S. T. Hess, and W. W. Webb. 2003. Imaging coexisting fluid domains in biomembrane models coupling curvature and line tension. *Nature.* 425:821–824.

43. Karatekin, E., O. Sandre, H. Guitouni, N. Borghi, P. H. Puech, and F. Brochard-Wyart. 2003. Cascades of transient pores in giant vesicles: line tension and transport. *Biophys. J.* 84:1734–1749.

44. Kuzmin, P. I., S. A. Akimov, Y. A. Chizmadzhev, J. Zimmerberg, and F. S. Cohen. 2005. Line tension and interaction energies of membrane rafts calculated from lipid splay and tilt. *Biophys. J.* 88:1120–1133.

45. Puech, P. H., N. Borghi, E. Karatekin, and F. Brochard-Wyart. 2003. Line thermodynamics: adsorption at a membrane edge. *Phys. Rev. Lett.* 90:128304.

46. Aritomi, M., N. Kunishima, N. Inohara, Y. Ishibashi, S. Ohta, and K. Morikawa. 1997. Crystal structure of rat Bcl-xL. Implications for the function of the Bcl-2 protein family. *J. Biol. Chem.* 272:27886–27892.

47. Muchmore, S. W., M. Sattler, H. Liang, R. P. Meadows, J. E. Harlan, H. S. Yoon, D. Nettesheim, B. S. Chang, C. B. Thompson, S. L. Wong, S. L. Ng, and S. W. Fesik. 1996. X-ray and NMR structure of human Bcl-xL, an inhibitor of programmed cell death. *Nature.* 381: 335–341.

48. Ludtke, S. J., K. He, W. T. Heller, T. A. Harroun, L. Yang, and H. W. Huang. 1996. Membrane pores induced by magainin. *Biochemistry.* 35:13723–13728.

49. Huang, H. W. 2000. Action of antimicrobial peptides: two-state model. *Biochemistry.* 39:8347–8352.

50. Shaw, J. E., J. R. Alattia, J. E. Verity, G. G. Prive, and C. M. Yip. 2006. Mechanisms of antimicrobial peptide action: studies of indolicidin assembly at model membrane interfaces by in situ atomic force microscopy. *J. Struct. Biol.* 154:42–58.

51. Munoz-Pinedo, C., A. Guio-Carrion, J. C. Goldstein, P. Fitzgerald, D. D. Newmeyer, and D. R. Green. 2006. Different mitochondrial intermembrane space proteins are released during apoptosis in a manner that is coordinately initiated but can vary in duration. *Proc. Natl. Acad. Sci. USA.* 103:11573–11578.